Progress In Electromagnetics Research C, Vol. 94, 131–144, 2019

Ultra Wide Band CPW Fed Patch Antenna with Fractal Elements and DGS for Wireless Applications

Anurima Majumdar*, Sisir K. Das, and Annapurna Das

Abstract—This article describes multiresonance behaviour to achieve ultra-wideband (UWB) characteristics of a co-planar waveguide (CPW) fed circular patch antenna with a ground plane reflector by using fractal elements and rectangular defective ground structure (RDGS) technique. The patch consists of a circular disc with six ring type fractal elements on the periphery of the disc and slotted defective ground surface (DGS) at the bottom of an FR4_epoxy dielectric substrate to increase the antenna bandwidth. The antenna resonates at frequencies of 5.4 GHz, 9 GHz, & 10.8 GHz with return loss better than −20 dB. The proposed antenna also exhibits UWB characteristics with (≤ -10 dB) impedance bandwidth of 170.4% in the frequency range from 1.8 GHz to 11 GHz. This covers the whole UWB range from 3.1 GHz to 10.6 GHz as defined by FCC. The antenna exhibits nearly omnidirectional radiation pattern and a gain ranging from 1 dBi to 6.8 dBi within the operating frequency range (1.8 GHz–11 GHz). An equivalent circuit model of the proposed antenna is developed, and the circuit response is obtained. All the measured results are found in good agreements with the simulated ones. The proposed antenna is suitable for applications in Wi-Fi, IEEE 802.11a Wireless LAN, WiMAX, ISM bands, wireless communications, etc.

1. INTRODUCTION

As per FCC, the UWB range is defined from 3.1 GHz to 10.6 GHz [1]. The ultra-wideband (UWB) patch antennas have advantages for its conformability, wideband operability, high data rate, low power consumption, robustness to fading, response to high speed pulses, small size, light weight, and low cost [1–5]. Many techniques have been reported in the literature for enhancing patch antenna bandwidth and multifrequency operation. One of the commonly used techniques is to configure the patch with fractal geometry [4–7]. Fractal elements are space-filling self-repeating structures that can be used in the form of Koch island, Sierpinski Carpet, Sierpinski gasket, Minkowski loop, Hilbert Curve, branches of tree, rough terrains, etc. In some recently published works Desai et al. [2] and Fallahi and Atlasbaf [3] used hexagonal shaped fractal geometries to obtain multiresonance and wideband response. The authors of both the papers used CPW feeding technique. Desai et al. [2] obtained a higher bandwidth of 135% after adding a defective ground structure which was better than that of [3]. Tripathi et al. [4] reported a hexagonal fractal antenna using Koch geometry for DGS and obtained a bandwidth of 122%. Ali et al. [7] proposed a miniaturized UWB antenna based on Sierpinski square slots and a defective ground structure. They reported a bandwidth of 124.7%. Many authors have used techniques other than fractal elements like loading of L-shaped slot and meandered line slots [8], edge tapering, and adding parasitic stubs [9], elliptic single complementary split-ring resonators (ESCSRRs) [10], split ring resonator [11], using of parasitic units [12, 13], step impedance resonator (SIR) [14, 15], to achieve multifrequency and UWB response. The usage of fractal elements is advantageous due to their behaviour as interconnected

Received 30 April 2019, Accepted 8 July 2019, Scheduled 22 July 2019

* Corresponding author: Anurima Majumdar (anurima.majumdar@gmail.com).

The authors are with the Department of Electronics and Communication Engineering, Guru Nanak Institute of Technology, JIS Group, Kolkata, West Bengal 700114, India.

capacitors & inductors and gives rise to different resonances which in turn results in high bandwidth, high gain, multi-frequency and multi-band response. Fractals have been applied to achieve multiband resonance, high gain, and high bandwidth [2–7, 16].

Another well-known and very much useful technique for wide impedance bandwidth or multi-frequency response is usage of a defective ground structure (DGS) [17, 18, 20–26]. When a defect in the ground plane is made, the current distribution at that plane gets disturbed. This discontinuity contributes in modified inductive and capacitive effect at the ground plane which in turn may produce additional resonant frequency. Hence the introduction of DGS enhances the antenna radiation characteristics and helps to reduce antenna size. A thorough insight of DGS along with analytical descriptions can be found in [17, 18]. The first DGS was reported as a dumbbell-shaped unit cell by Park et al. [19]. Guha et al. [17] described different shapes of DGS viz. spiral shaped, fractal, half circle, V-shaped, split ring resonators, etc. A periodic DGS consisting of 5 dumbbell-shaped nonuniform slots in the ground plane was reported by Liu et al. [20] which exhibits a bandwidth of 4.26 GHz. Weng et al. [21] also gave different analytical models for DGS. The DGS can be equivalent to a larger capacitance, and its uses can also enhance gain as it can reduce surface waves [22]. Kazerooni and Cheldavi [23] proposed a wideband multi-ring fractal antenna that exhibited an impedance bandwidth of 64%.

Many authors have discussed different approaches to develop equivalent circuit of microstrip patch antenna [24, 25]. Nashaat et al. described an equivalent circuit of a patch antenna with rectangular DGS where the slot was presented through a simple L-C resonator [26].

The present paper describes a new configuration of patch antenna to obtain Tri-frequency response in UWB range with high impedance bandwidth of 170.4%. In this design, six small circular ring elements are added to the periphery of a circular patch on an FR4_epoxy dielectric substrate of $\varepsilon_r = 4.4$ & thickness $h = 1.6$ mm as shown in Figure 1(a). The configuration is analysed using HFSS software. When a continuous ground plane is used, four resonant frequencies at 5.4 GHz, 6 GHz, 9.5 GHz, & 10.8 GHz with a bandwidth of 105% are obtained with band rejection characteristics in the frequency range from 7.5 GHz to 9.3 GHz as shown in Figure 2.

A metallic plane below the substrate is used as reflecting plane which contributes to achievement of high bandwidth and gain of the antenna and enhance unidirectional radiation. After making the reflector ground plane defective with a narrow rectangular slot (Figure 1(b)), the ≤ -10 dB bandwidth is further enhanced from 105% to 170.4%. The configuration of the antenna with rectangular slotted ground structure (RDGS) is analysed using HFSS software. This modified antenna resonates at three resonating frequencies, i.e., 5.4 GHz, 9 GHz, & 10.8 GHz with much better return loss -45.7 dB, -43.2 dB, and -27.89 dB, respectively, with impedance bandwidth of 170.4% in the frequency range from 1.8 GHz to 11 GHz. All the important parameters that control the bandwidth and impedance matching are described in Section 3.

The next part of the paper concentrates on developing an equivalent circuit model of the CPW-fed proposed patch antenna with RDGS. The circuit simulation is done using NI AWR Software tool. The S_{11}, gain and radiation pattern of the antenna are computed theoretically and also measured using Vector Network Analyzer. All the results are found in good agreement with each other.

2. DESIGN OPTIMIZATION OF THE ANTENNA CONFIGURATION

The geometrical configuration of the proposed antenna with RDGS is shown in Figure 1. It consists of a CPW-fed circular disc of radius $r = 9.5$ mm in the form of a monopole. There is a ground plane reflector with narrow slot (Figure 1(b)) below the substrate. The circular disc is designed using the formula [27] of resonant frequency,

$$f_r = \frac{x'_{mn}c}{2\pi r\sqrt{\varepsilon_r}} \tag{1}$$

For TM_{110} mode $x'_{mn} = 1.841$, $c = 3 \times 10^8$ m/sec. The antenna is designed on an FR4_epoxy substrate having $\varepsilon_r = 4.4$ and thickness $h = 1.6$ mm. The resonant frequency $f_r = 4.5$ GHz for radius $r = 9.5$ mm. This is the specification of the initial single circular patch antenna without any fractal elements. After introduction of fractal elements, the resonant frequency shifts to 5.4 GHz with additional resonance at frequencies 9 GHz and 10.8 GHz.

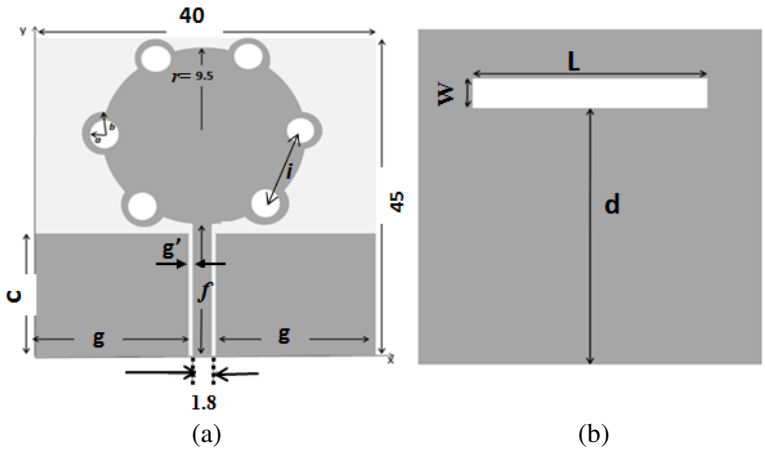

Figure 1. (a) CPW fed patch with fractal elements, (b) RDGS configuration.

The gap between the coplanar waveguide and the feedline is g'. Six fractal elements in the form of small annular rings, each with inner radius a & outer radius b, are symmetrically introduced at the periphery of the disc. The linear distance from one fractal element to anothe is $i = 9.95\,\text{mm}$. The configuration is printed on an FR4_epoxy substrate with $\varepsilon_r = 4.4$ and thickness $h = 1.6\,\text{mm}$. The size of the ground plane is $40\,\text{mm} \times 45\,\text{mm}$. The ground plane is modified with a narrow rectangular slot of dimension $L\,\text{mm} \times W\,\text{mm}$ at the bottom of the dielectric substrate. The distance of the rectangular slot on the ground from the feed end is d.

The proposed antenna is simulated using Ansoft HFSS software. Several iterations are attempted by changing the inner radius (a) of the fractal ring and CPW feed length (c). The tuning of the dimensions of rectangular DGS slot helps in improving the ($\leq -10\,\text{dB}$) impedance bandwidth to 170.4%. The antenna covers three resonance frequencies at 5.4 GHz, 9 GHz, & 10.8 GHz with return losses $-45.7\,\text{dB}$, $-43.2\,\text{dB}$, and $-27.89\,\text{dB}$, respectively. The gap (g') between the coplanar ground plane and feed line is a very important parameter for affecting the impedance bandwidth. In this paper, the optimum size of the gap is 0.6 mm for the best impedance matching. The gain for the entire range of operating frequency (1 GHz–13 GHz) shows an increase in nature starting from 1.08 dBi to 6.8 dBi. Details of result obtained are described below.

3. RESULTS & DISCUSSION

The results for return loss vs. frequency, radiation pattern, & gain characteristics of the configurations of the antenna obtained using Ansoft HFSS software tool and measurements with vector network analyser are graphically shown in Figures 2–11.

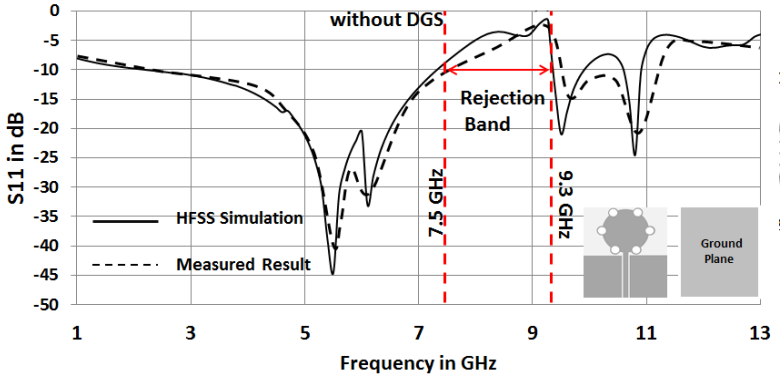

Figure 2. Simulated and measured S_{11} vs. frequency for the antenna without DGS.

3.1. S_{11} Characteristics without DGS

Figure 2 shows the frequency vs. S_{11} response of the antenna configuration without DGS. The iteration of the simulation without RDGS shows an impedance bandwidth of 105% covering resonance frequencies at 5.4 GHz, 6 GHz, 9.5 GHz, and 10.8 GHz with return losses −45 dB, −32 dB, −20 dB, and −25 dB, respectively. There is a rejection band from 7.5 GHz to 9.3 GHz. The return loss is experimentally verified and shown in Figure 2. The measured and simulated values are well matched.

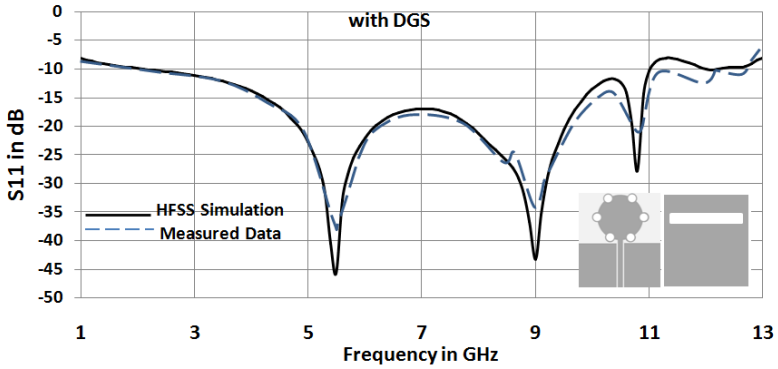

Figure 3. Simulated and measured result of S_{11} vs. frequency for the antenna with RDGS.

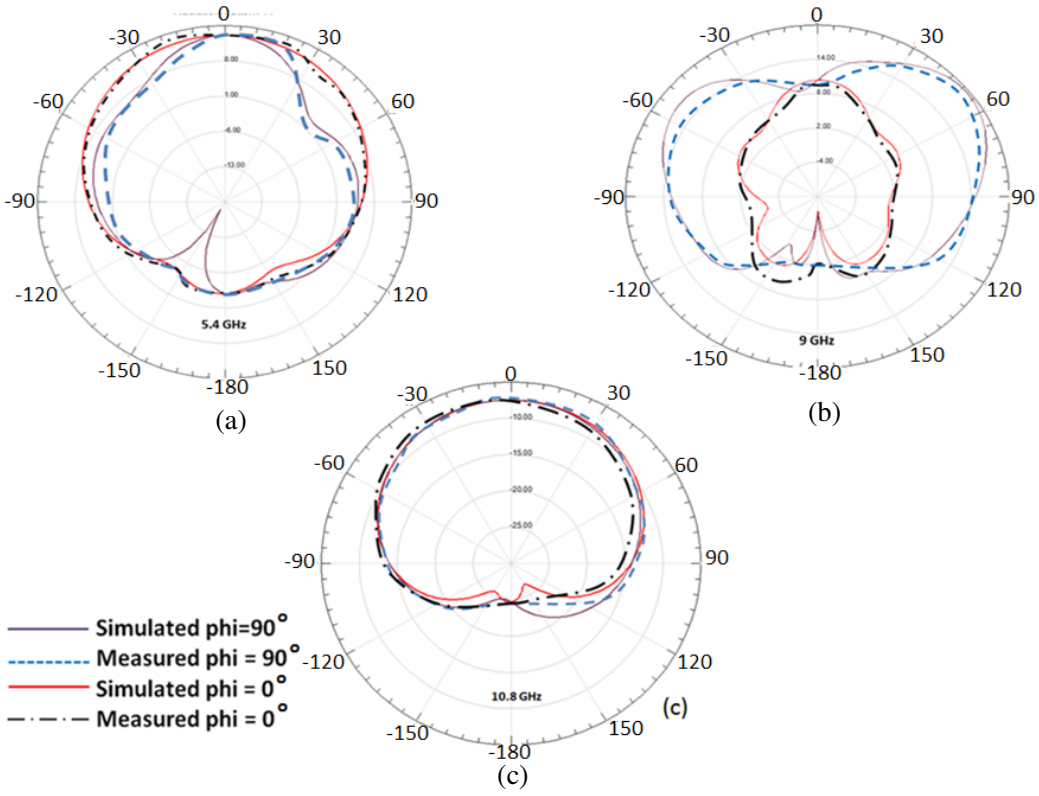

Figure 4. Simulated and measured radiation patterns at (a) 5.4 GHz (b) 9 GHz (c) 10.8 GHz.

3.2. S_{11} Characteristics with RDGS

The antenna is modified by using defective ground plane where a rectangular narrow slot (RDGS) is cut in the metallic ground plane reflector as shown in Figure 1(b). All the dimensions of the patch and

fractal elements are optimized in order to obtain the best performance.

The final design specifications for the configuration of Figure 1 are: substrate $\varepsilon_r = 4.4$ with height 1.6 mm, *ground plane size 40 mm × 45 mm;* $a = 1.8$ *mm,* $b = 2$ *mm,* $c = 24$ *mm,* $d = 36$ *mm,* $f = 25.5$ *mm,* $g = 18.5$ *mm,* $g' = 0.6$ *mm,* $i = 9.95$ *mm,* $r = 9.5$ *mm,* $L = 32$ *mm,* $W = 2$ *mm.*

This modified antenna increases the bandwidth to 170.4% in the frequency range from 1.8 GHz to 11 GHz which covers the entire UWB range (3.1 GHz–10.6 GHz). The best impedance matching is found at resonance frequencies 5.4 GHz, 9 GHz, & 10.8 GHz with return losses −45.7 dB, −43.2 dB, and −27.89 dB. The simulated and measured results are shown in Figure 3. Therefore, the CPW-fed circular patch with fractal ring elements and RDGS produces better performance for further study.

Radiation patterns of this configuration at each resonance frequencies are determined using Ansoft HFSS Software Tool, and the results are shown in Figure 4. The measured and simulated results are found in good agreement.

A little variation in the measurement results is observed which is due to fabrication, soldering effect, and SMA connector losses.

4. PARAMETRIC STUDY OF THE PROPOSED ANTENNA WITH RDGS

All the parameters of the configuration, which control the bandwidth, resonance frequencies and impedance matching, are elaborately discussed in this section, and results are shown in Figures 5–10. In each case, the individual parameters are shown by enclosing the region with dotted lines. The gap between the coplanar waveguide plane and feedline is a controlling parameter for impedance bandwidth and frequency matching. As the gap increases, the coupling capacitance changes, and the impedance bandwidth becomes narrow [2]. For the proposed antenna, the gap, g', is optimized to 0.6 mm. In Figure 5(a), the antenna performance for different g' is shown. In Figure 5(b), the effect of the length, c, of CPW plane is shown. It is observed that the impedance bandwidth and resonant frequencies change considerably with the change in the length of CPW. A relation between the bandwidth and CPW length 'c' can be expressed by Equation (2) which is obtained by curve fitting and iterative techniques using MATLAB.

$$\text{Bandwidth} = -41662 + 5727c - 262c^2 + 4c^3 \tag{2}$$

The best tuning of frequency and impedance bandwidth (≤ -10 dB) is found for CPW length of $c = 24$ mm.

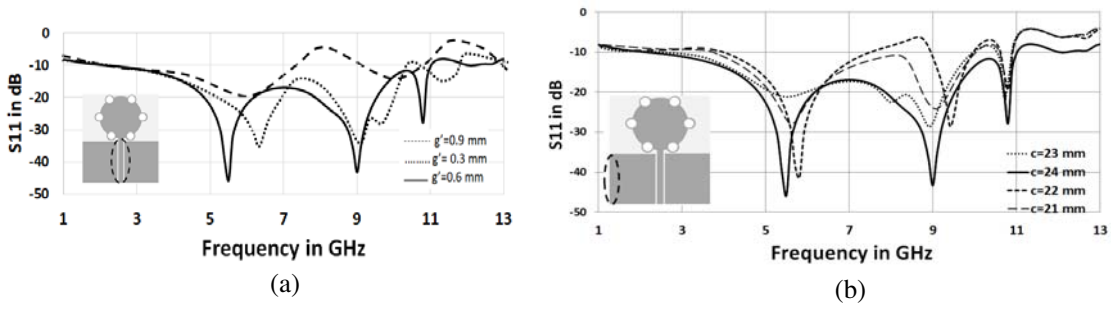

Figure 5. Effect of the CPW parameters on antenna performance. (a) Gap between CPW plane and feedline, g'. (b) CPW plane length, c.

Another important parameter that affects the performance is the inner radius (a) of the ring-shaped fractal elements. It mostly affects the impedance matching and bandwidth as shown in Figure 6 for different $\boldsymbol{a}$ of the ring elements. The curve fitting and iteration technique is used through MATLAB to find the relation between bandwidth and inner radius which is expressed below,

$$\text{Bandwidth} = 5685 - 12334a + 8658a^2 - 1949a^3 \tag{3}$$

The optimized performance is achieved with the inner radius, $a = 1.8$ mm, where the outer radius, b, is kept constant as $b = 2$ mm.

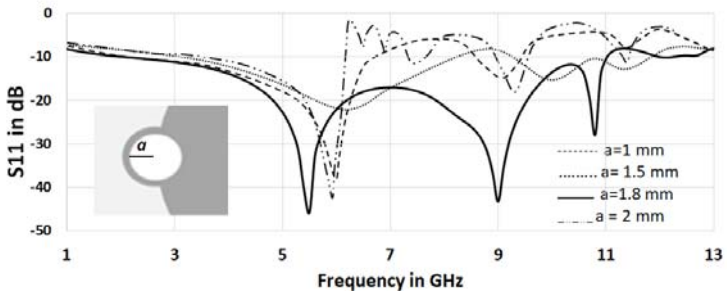

Figure 6. Effect of the ring-shaped fractal element dimension (inner radius, a) on antenna performance.

In Figures 7(a)–(h), the current distribution on the metallic ground plane reflector and radiating patch is shown for resonant frequencies 5.4 GHz and 10.8 GHz. In the figures, the surface current density and direction of current flow are observed. The current distribution at the bottom ground surface is discontinued by the introduction of the RDGS structure (Figures 7(d), (h)). The current distribution at 10.8 GHz is given in Figures 7(e)–(h) to show the effect of slot on the ground plane. The position of the slot for RDGS is selected according to the current distribution. The dimension of the slot is 32 mm × 2 mm for the best antenna performances. The comparative results are shown in Figures 8 and 9.

In the proposed antenna, it has been observed that the distance d of the DGS from feed point affects the bandwidth to a great extent as shown in Figure 8, where d is varied from 20 mm to 40 mm, and the best performance is obtained for $d = 36$ mm. The relation between bandwidth and d is shown in Equation (4).

$$\text{Bandwidth} = 117 + (68 - 116.7)/(1 + (d/33)^{89}) \tag{4}$$

Figure 9 shows the effect of dimension of the RDGS on antenna performance. It has been observed that

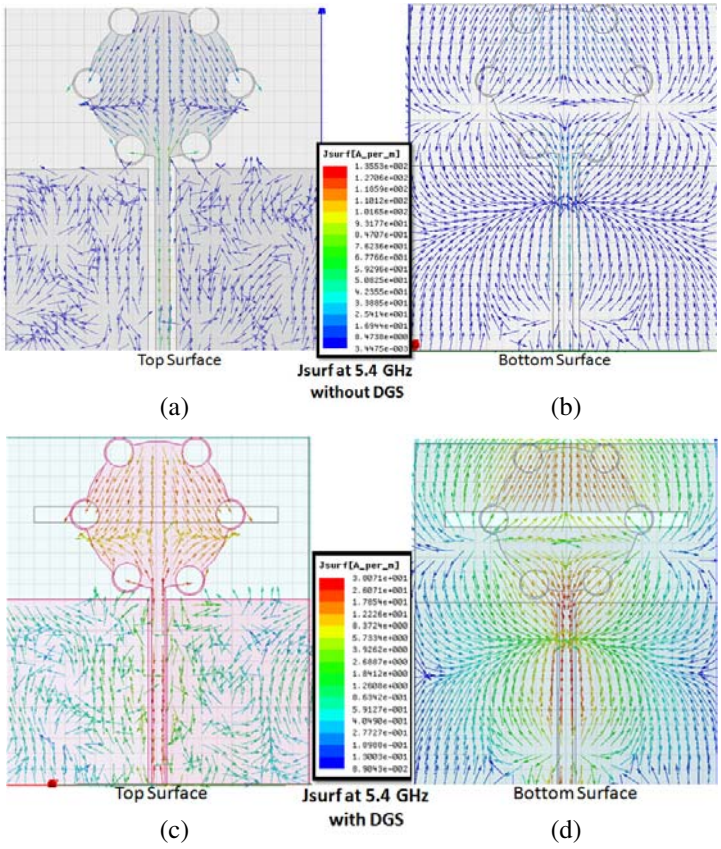

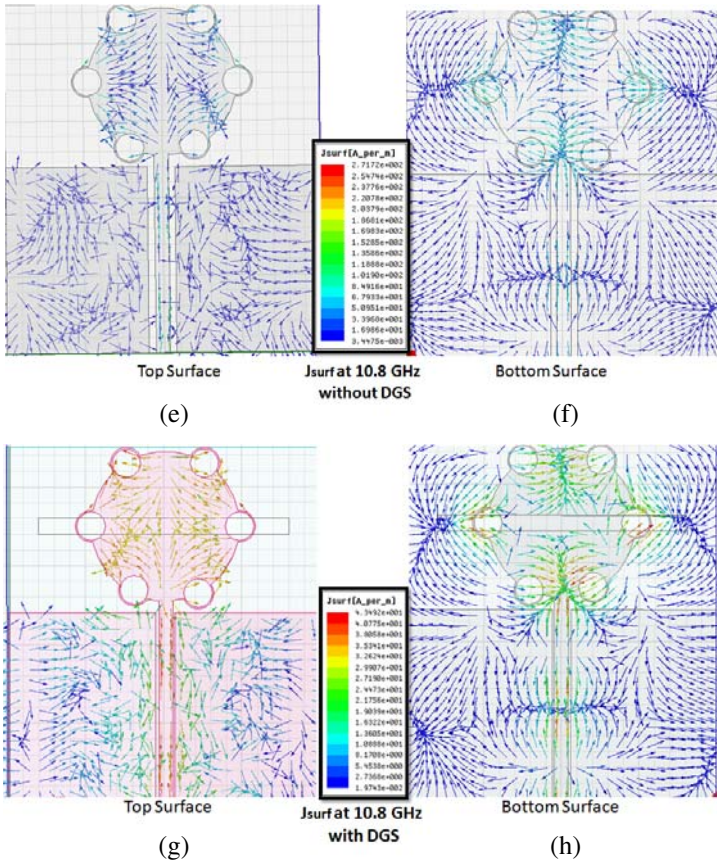

Figure 7. The current distribution at 5.4 GHz without RDGS. (a) Top surface. (b) Bottom surface. The current distribution at 5.4 GHz with RDGS. (c) Top surface. (d) Bottom surface. Current distribution at 10.8 GHz without RDGS. (e) Top surface. (f) Bottom surface. Current distribution at 10.8 GHz with RDGS. (g) Top surface. (h) Bottom surface.

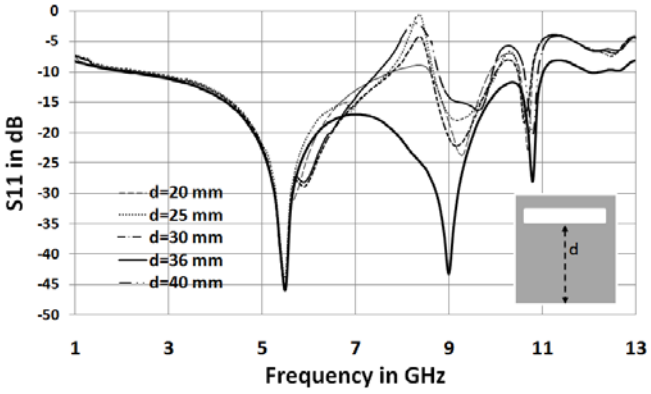

Figure 8. The effect of the distance, d of the DGS (rectangular slot) from feed point.

with the change in L the bandwidth is reduced. As the width (W) of the slot changes a shift in resonant frequencies can be seen. The gain of the antenna is found increasing for the entire UWB range from 1 dBi to a maximum value of 6.8 dBi. The frequency vs. gain plot is shown in Figure 10. An antenna with a gain more than 3 dBi is considered a good radiator [2].

The surface current distributions at three resonant frequencies of 5.4 GHz, 9 GHz, & 10.8 GHz are shown in Figures 11(a)–(c). It can be seen that the surface current density is concentrated on the lower

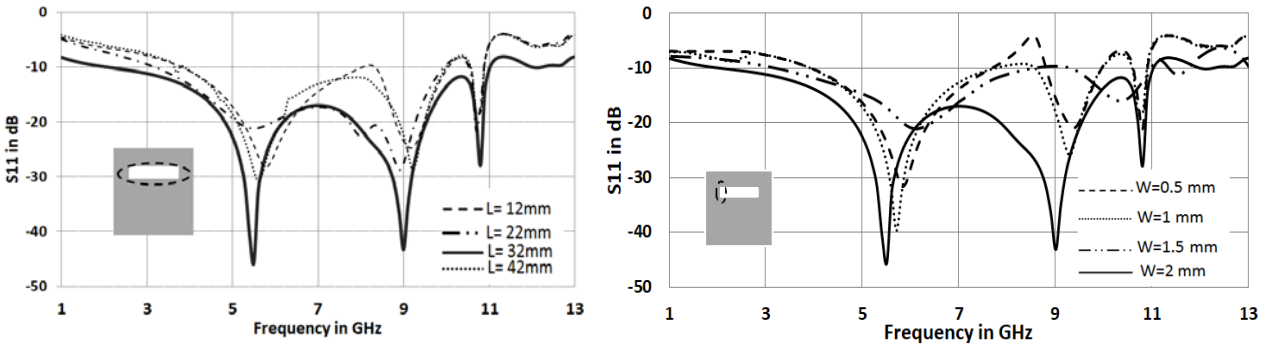

(a) (b)

Figure 9. Effect of the dimensions of the rectangular slot as the defective ground structure on antenna performance (a) Length, L (b) Width, W.

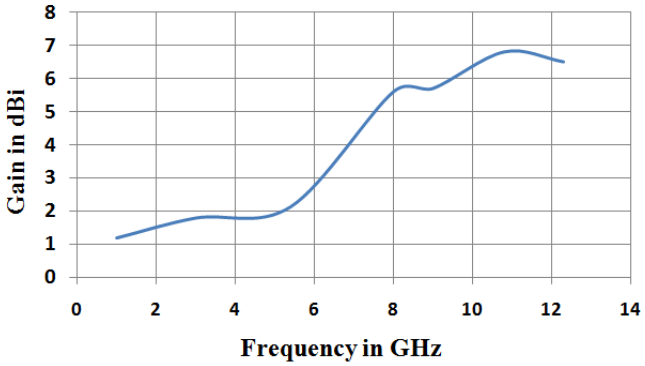

Figure 10. The Gain vs. Frequency of the proposed antenna.

edge of the radiator and around the fractal elements. This means that the lower part of the antenna and fractal elements affects the impedance characteristics for all the frequencies. Current density is also higher around all the fractal elements than centre region. Therefore, it is concluded that the dimensions of the fractal elements are very much influential for radiation characteristics of the proposed antenna.

5. DEVELOPMENT OF EQUIVALENT CIRCUIT FOR THE PROPOSED ANTENNA

The equivalent circuit of the proposed antenna is obtained using AWR Design Environment-14 as shown in Figure 12(a). In Figure 12(b), the circuit is shown in simplified form. The impedance model approach [24–26] is followed to develop the equivalent circuit. The input port is excited with a 50 Ohm RF source. In the circuit L_{feed} is used to represent the feed inductance, and C_{patch} is used to represent the antenna static capacitance. The impedance of the circular patch is represented by Z_p. The peripheral ring fractal elements are represented by L-C resonator circuits connected in shunt (marked Z_{slot}). In UWB antennas wideband impedance matching can be achieved through several adjacent resonances of parallel resonators connected in series [25] as shown in Figure 12(a). This introduces a discontinuity represented by LC resonator circuit (marked Z_{freq}). The coupling between ground plane and radiating patch is represented by a coupling capacitor, C_{in}, at the input end. The RDGS in the reflecting ground plane is shown as Z_d in the equivalent circuit model. The output port is terminated with a 50 Ω load for impedance matching with the input port.

The admittance for the peripheral rings can be expressed as:

$$Y_{slot} = j\omega \left(\sum_{k=1}^{n} C_k - \frac{1}{\omega^2} \sum_{k=1}^{n} \frac{1}{L_k} \right) \tag{5}$$

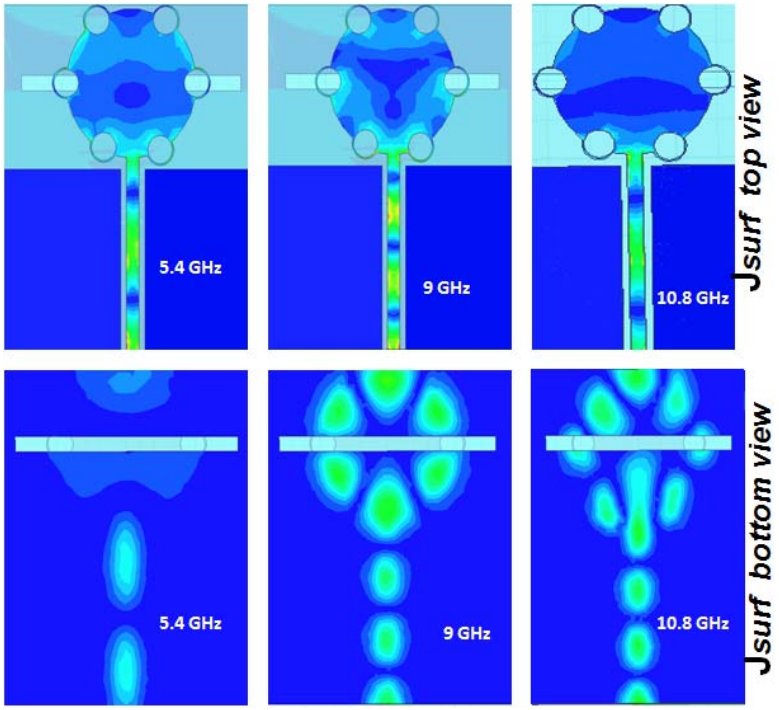

Figure 11. Surface current distribution of the proposed antenna at (a) 5.4 GHz (b) 9 GHz (c) 10.8 GHz.

Here $n(=6)$ is the number of fractal rings. The admittance for the patch is given by

$$Y_p = \frac{1}{j\omega L_p} + j\omega C_p \tag{6}$$

From Eqs. (5)–(6) we get

$$Z_{p\text{-}slot} = \frac{1}{Y_p} + \frac{1}{Y_{slot}} \tag{7}$$

The admittances and impedances of each parallel resonance circuit representing three resonance peaks can be expressed as

$$Y_a = G_a + \frac{1}{j\omega L_a} + j\omega C_a; \quad Z_a = \frac{1}{Y_a} \tag{8}$$

$$Y_b = G_b + \frac{1}{j\omega L_b} + j\omega C_b; \quad Z_b = \frac{1}{Y_b} \tag{9}$$

$$Y_c = G_c + \frac{1}{j\omega L_c} + j\omega C_c; \quad Z_c = \frac{1}{Y_c} \tag{10}$$

The total impedance can be expressed as

$$Z_{freq=} Z_a + Z_b + Z_c + 50 \tag{11}$$

The impedance of the slot in the ground plane is,

$$Z_d = j\omega L_d + \frac{1}{j\omega C_d} \tag{12}$$

From Equations (6), (7), & (12) we get,

$$Z_L = \frac{(Z_P + Z_{Slot}) \cdot Z_d}{Z_p + Z_{slot} + Z_d} \tag{13}$$

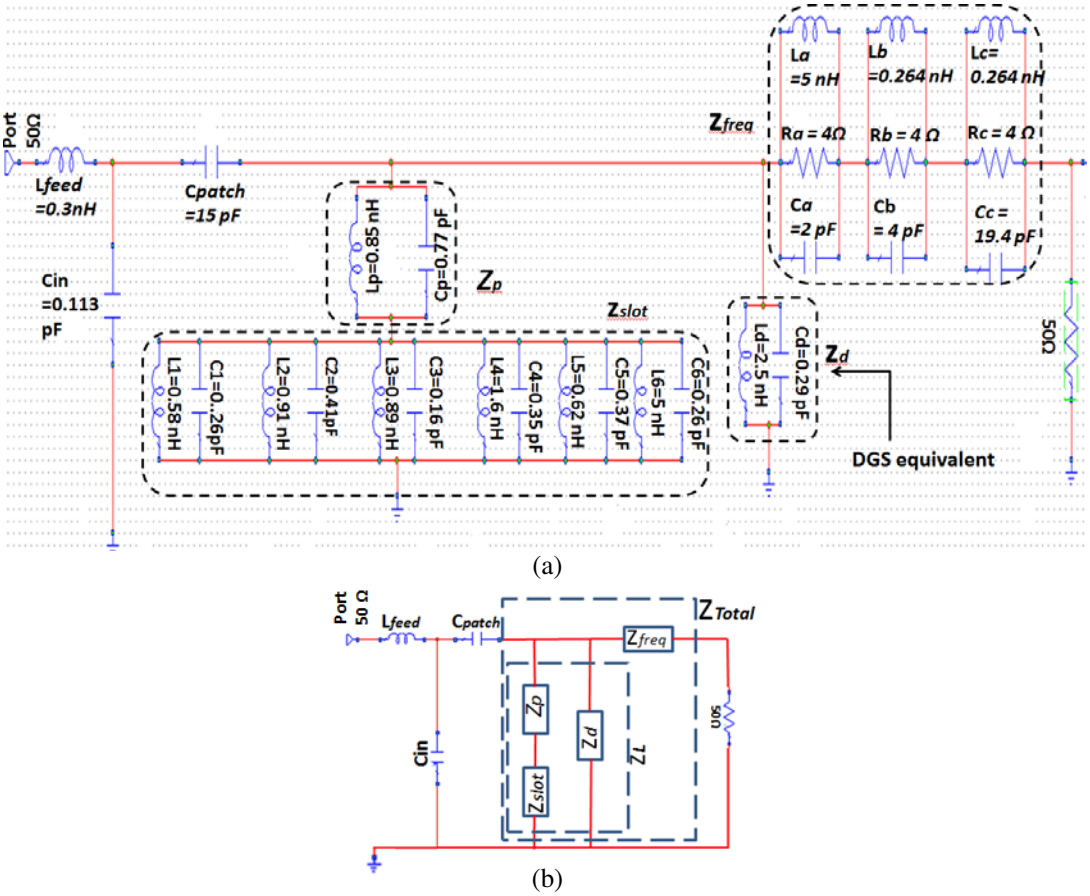

Figure 12. (a) Equivalent circuit model of the proposed antenna as simulated by AWR Design Environment-14 circuit simulator. (b) Simplified equivalent circuit.

The total impedance from Equations (11)–(13) is,

$$Z_{Total} = \frac{Z_L \cdot Z_{freq}}{Z_L + Z_{freq}} \tag{14}$$

The impedance of C_{patch} is,

$$Z_{patch} = \frac{1}{j\omega C_{patch}} \tag{15}$$

The total impedance from Equations (14)–(15) is,

$$Z_T = \left(Z_{Total} + \frac{1}{j\omega C_{patch}} \right) \tag{16}$$

Therefore, the impedance of the whole equivalent circuit can be expressed as,

$$Z_{eq} = j\omega L_{feed} + \left[\frac{Z_T \cdot \frac{1}{j\omega C_{in}}}{Z_T + \frac{1}{j\omega C_{in}}} \right] \tag{17}$$

The input reflection coefficient from the circuit is given by,

$$S_{11} = \frac{Z_{eq} - 50}{Z_{eq} + 50} \tag{18}$$

By iteration process all circuit elements are evaluated for which the S_{11} parameter is computed from Equation (18). The simulated and measured values are found in good agreement.

By using curve fitting and iterative techniques, the values of circuit component are selected and shown in Table 1.

Table 1. (inductors in nH, capacitors in pF and resistors in ohm).

L_{feed}	C_{patch}	C_{in}	C_1	L_1	C_2	L_2	C_3	L_3	C_4	L_4	C_5	L_5	C_6	L_6
0.3	15	0.113	0.26	0.58	0.41	0.9	0.16	0.9	0.35	1.6	0.37	0.62	0.26	5
L_a	C_a	L_b	C_b	L_c	C_c	L_d	C_d	L_p	C_p	$R_a=R_b=R_c$				
5	2	0.264	4	0.26	19.4	2.5	0.29	0.85	0.77	4				

From the above discussion it may be concluded that by changing the design parameters of the ring resonators, CPW and RDGS, the values of equivalent inductance and capacitance may be controlled which will result in improved resonant frequency for matching and wider bandwidth. The comparison of S_{11} response between HFSS simulation, the equivalent circuit simulation, measurement result, & calculated values is shown in Figure 13. All the results are found in good agreement with each other. The hardware design of the proposed antenna and experimental setup are shown in Figures 14(a)–(c).

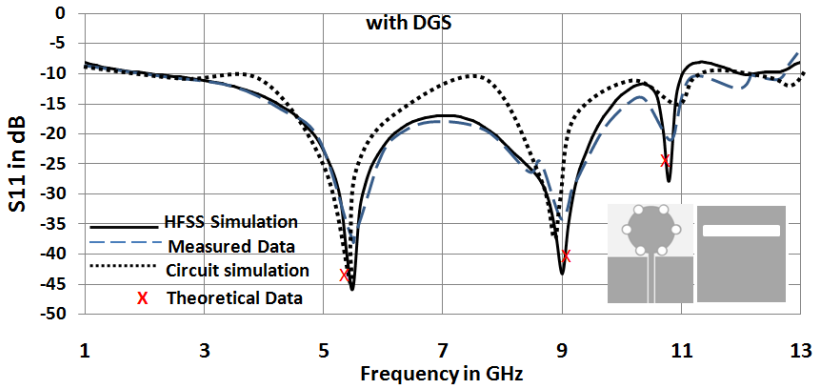

Figure 13. Comparative study of S_{11} response between HFSS simulation, equivalent circuit simulation, measured data and data obtained from the calculation.

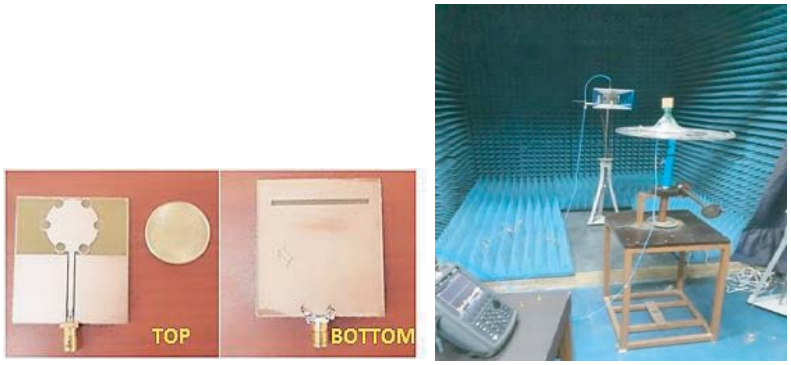

(a) (b) (c)

Figure 14. (a)–(b) Hardware design. (c) The experimental set up.

The designed antenna is applicable to wireless communication, IEEE 802.11a Wireless LAN, WiMAX, Wi-fi, wireless sensor networks, ISM band applications, etc.

5.1. Comparison with Recent Works

The proposed antenna is much simpler to design with respect to some recent reported works [2–4, 7, 13] and gives better bandwidth and return losses. The basic construction of the antenna is inspired from the work reported in [2, 3]. The below mentioned Table 2 shows the comparative study of the proposed structure with some recent relevant works.

Table 2. Comparative performance analysis of the proposed antenna with recenly published works.

Antenna Design	Dimension (mm)	Bandwidth (%)	Highest achieved Gain (dBi)	S11 (dB)	Resonant Frequency (GHz)
Proposed antenna	$45 \times 40 \times 1.6$	170.4%	6.8	-45.7 -43.2 -27.89	5.4 9 10.8
Desai et al. [2]	$45 \times 40 \times 1.6$	135%	6.8	-25.02 -26.03	3.79 5.5
Fallahi and Atlasbaf [3]	$25 \times 25 \times 1$	113.35%	3.4	-55 -27 -30	4 7 10
Tripathi et al. [4]	$31 \times 28 \times 1.6$	122%	6.2	-25 -45 -25	4.3 7.2 10
Ali et al. [7]	$28 \times 28 \times 1.6$	127.3%	5.95	-19 -40 -32	5.95 8.8 12.5
Kazerooni and Cheldavi [23]	$126 \times 112 \times 0.663$	64%	–	< -20 dB	6 9 12 14

6. CONCLUSION

A technique to design a CPW-fed ultra-wideband patch antenna with fractal elements and a metallic ground plane reflector with defective ground structure has been carried out for wireless communication applications. To obtain desired performance by the antenna, six rings shaped fractal elements are added at the peripheral edge of the patch, and a rectangular slot is cut into the ground plane reflector. Further improvement is observed when the length, width, and the distance of the RDGS from the feed point are varied and optimized to get the best performance. The inner radius of the fractal elements also affects the performance of the antenna. The CPW length and the gap between the CPW plane and feedline are also optimized for better performance. The measured results show good agreement with the simulation and equivalent circuit model. The proposed antenna resonates at three frequencies, i.e., 5.4 GHz, 9 GHz, & 10.8 GHz in the frequency range of 1.8 GHz to 11 GHz. The calculated return losses are -45.7 dB, -43.2 dB, and -27.89 dB at the resonant frequencies, respectively. The impedance bandwidth is found to be 170.4% which covers the entire UWB range with a maximum gain of 6.8 dBi. The dimension, impedance bandwidth, highest achieved gain, S_{11}, and peak resonant frequencies of the proposed antenna are compared with earlier published works. The performance of the proposed antenna is found better than that of others.

ACKNOWLEDGMENT

The authors acknowledge the Department of Electronics & Telecommunication Engineering, Jadavpur University for providing their Laboratory facility for the measurement of the antenna.

REFERENCES

1. FCC, "FCC 1st report and order on ultrawideband technology," Washington, DC, 2002.
2. Desai, A., T. Upadhyaya, R. Patel, S. Bhatt, and P. Mankodi, "Wideband high gain fractal antenna for wireless applications," *Progress In Electromagnetics Research Letters*, Vol. 74, 125–130, 2018.
3. Fallahi, H. and Z. Atlasbaf, "Bandwidth enhancement of a CPW-fed monopole antenna with small fractal elements," *AEU-International Journal of Electronics and communications*, Vol. 69, No. 2, 590–595, 2015.
4. Tripathi, S., A. Mohan, and S. Yadav, "Hexagonal fractal ultra-wideband antenna using Koch geometry with bandwidth enhancement," *IET Microw. Antennas Propag.*, Vol. 8, No. 15, 1445–1450, 2014.
5. Anguera, J., C. Puente, V. Borja, and J. Soler, "Fractal-shaped antennas: A review," *Wiley Encycl. RF Microw. Eng.*, Vol. 2, 1620–1635, 2005.
6. Haji-Hashemi, M. R., M. Mir-Mohammad Sadeghi, and V. M. Moghtadai, "Space-filling patch antennas with CPW feed," *PIERS Online*, Vol. 2, No. 1, 69–73, Mar. 2006.
7. Ali, T., B. K. Subhash, and C. B. Rajashekhar, "A miniaturized decagonal Sierpinski UWB fractal antenna," *Progress In Electromagnetics Research C*, Vol. 84, 161–174, 2018.
8. Brar, R. S. and S. K. Sharma, "A triple-band dipole antenna for UMTS/LTE and UWB," *Applications, International Journal of Electronics Letters*, 2017.
9. Sharan, R. K., S. K. Sharma, A. Gupta, and R. K. Chaudhary, "An edge tapered rectangular patch antenna with parasitic stubs and slot for wideband applications," *Wireless Pers. Commun.*, Springer Science + Business Media, New York, 2015.
10. Sarkar, D., K. V. Srivastava, and K. Saurav, "A compact microstrip-fed triple band-notched UWB monopole antenna," *IEEE Antennas and Wireless Propagation Letters*, Vol. 13, 2014.
11. Sharma ,S. K. and C.-W. Park, "A dual band-notched ultra wideband antenna using split ring resonators," *2016 URSI Asia-Pacific Radio Science Conference (URSI AP-RASC)*, 2016.
12. Siddiqui, J. Y., C. Saha, C. Sarkar, et al., "Ultra-wideband antipodal tapered slot antenna with integrated frequency notch characteristics," *IEEE Transactions on Antennas and Propagation*, Vol. 66, No. 3, 1534–1539, 2018.
13. Shaik, L. A., C. Saha, Y. Antar, et al., "An antenna advances for cognitive radio: Introducing a multilayered split ring resonator-loaded printed ultra-wideband antenna with multifunctional characteristics," *IEEE Antennas & Propagation Magazine*, Vol. 1, 20–33, 2018.
14. Zhang, J., T. Chen, Y. Lv, and H. Xing, "A practical CPW-fed UWB antenna with reconfigurable dual band-notched characteristics," *Progress In Electromagnetics Research M*, Vol. 81, 117–126, 2019.
15. Zhang, X.-M., J. Ma, C.-X. Li, A.-S. Ma, Q. Wang, and M.-X. Shao, "A new planar monopole UWB antenna with quad notched bands," *Progress In Electromagnetics Research Letters*, Vol. 81, 39–44, 2019.
16. Bilal, M. H., A. A. Rahim, H. Maab, and M. M. Ali, "Modified wang shaped ultra-wideband (UWB) fractal patch antenna for millimetre-wave applications," *2018 Progress In Electromagnetics Research Symposium (PIERS — Toyama)*, 280–284, Japan, Aug. 1–4, 2018.
17. Guha, D., S. Biswas, and Y. M. M. Antar, *Defected Ground Structure for Microstrip Antennas, in Microstrip and Printed Antennas: New Trends, Techniques and Applications*, John Wiley & Sons, London, UK, 2011.
18. Khandelwal, M. K., B. K. Kanaujia, and S. Kumar, "Defected ground structure: Fundamentals, analysis, and applications in modern wireless trends," *International Journal of Antennas and Propagation*, Vol. 2017, Article ID 2018527, 22 pages, 2017.

19. Park, J.-I., C.-S. Kim, J. Kim et al., "Modelling of a photonic band-gap and its application for the low-pass filter design," *Proceedings of the Asia Pacific Microwave Conference (APMC'99)*, Vol. 2, 331–334, Nov.–Dec. 1999.
20. Liu, H. W., Z. F. Li, X. W. Sun, and J. F. Mao, "An improved 1-D periodic defected ground structure for microstrip line," *IEEE Microwave and Wireless Components Letters*, Vol. 14, No. 4, Apr. 2004.
21. Weng, L. H., Y. C. Guo, X. W. Shi, and X. Q. Chen, "An overview on defected ground structure," *Progress In Electromagnetics Research B*, Vol. 7, 173–189, 2008.
22. Geng, J. P., J. J. Li, R. H. Jin, S. Ye, X. L. Liang, and M. Z. Li, "The development of curved microstrip antenna with defected ground structure," *Progress In Electromagnetics Research*, Vol. 98, 53–73, 2009.
23. Kazerooni, M. and A. Cheldavi, "Design and fabrication of wide band printed multi-ring fractal antenna for commercial applications," *PIERS Proceedings*, Beijing, China, Mar. 23–27, 2009.
24. Meena, M. L., M. Kumar, G. Parmar, and R. S. Meena, 'Design analysis and modelling of directional UWB antenna with elliptical slotted ground structure for applications in C- & X-bands," *Progress In Electromagnetics Research C*, Vol. 63, 193–207, 2018.
25. Pele, I., A. Chousseaud, and S. Toutain, "Simulation modelling of impedance and radiation pattern antenna for UWB pulse modulation," *Proc. IEEE AP-S Int. Symp.*, Vol. 2, 1871–1874, Jun. 2004.
26. Nashaat, D., H. A. Elsadek, E. Abdallah, H. Elhenawy, and M. F. Iskander, "Electromagnetic analyses and an equivalent circuit model of microstrip patch antenna with rectangular defected ground plane," *2009 IEEE Antennas and Propagation Society International Symposium*, 1–4, Charleston, SC, 2009.
27. Garg, R., *Microstrip Antenna Design Handbook*, Artech House, 2001.